BRAGE/IMR

Brage IMR –

Havforskningsinstituttets institusjonelle arkiv

Dette er forfatters siste versjon av den fagfellevurderte artikkelen, vanligvis omtalt som postprint. I Brage IMR er denne artikkelen ikke publisert med forlagets layout fordi forlaget ikke tillater dette. Du finner lenke til forlagets versjon i Brage-posten.
Det anbefales at referanser til artikkelen hentes fra forlagets side.

Ved lenking til artikkelen skal det lenkes til post i Brage IMR, ikke direkte til pdf-fil.

Brage IMR –

Institutional repository of the Institute of Marine Research

This is the author's last version of the article after peer review and is not the publisher's version, usually referred to as postprint. You will find a link to the publisher's version in Brage IMR. It is recommended that you obtain the references from the publisher's site.

Linking to the article should be to the Brage-record, not directly to the pdf-file.

HAVFORSKNINGSINSTITUTTET
INSTITUTE OF MARINE RESEARCH

Foto: Leif Nøttestad

Estimating tail-beat frequency using split-beam echosounders

Nils Olav Handegard[a] Geir Pedersen[a], and Ole Brix[b,c]

Handegard, N.O., Pedersen, G., and Brix, O. 2009. Estimating tail-beat frequency using split-beam echosounders – ICES Journal of Marine Science, 69: 000–000.

Data from a standard split-beam echosounder are used to estimate tail-beat frequency within a dense herring (*Clupea harengus* L.) layer. The data were collected by lowering a horizontally projecting 38 kHz split-beam transducer into a herring layer at 245 m depth. Individual targets were concatenated into tracks, and a fast Fourier transform was used to estimate the periodogram of the backscattering strengths along each track. A simple model, assumed accurate under certain conditions, was used to relate the periodogram to tail-beat frequency. The requisite conditions are discussed. Presented are examples of accurate tail-beat estimates from single high-quality tracks, which are consistent with statistics on all tracks in the test data set. Further, the cross-periodogram between closely spaced individuals is calculated on selected tracks to estimate the relative phase between the adjacent tracks within the school. Finally, discussed are the potential uses of this method to resolve schooling behaviour, improve target strength estimates, and even estimate fish condition.

Keywords: Fish swimming, split-beam echosounder, tail-beat frequency, target tracking

Running Heads: Estimating tail-beat frequency

Filled in by Editor: Received 7 August 2008; Accepted .

[a] *Institute for Marine Research, PO Box 1870 Nordnes, 5817 Bergen, Norway.*
[b] *Department of Biology, University of Bergen, PO Box 7800, 5020 Bergen, Norway.*
[c] *The Michelsen Centre for Industrial Measurement Science and Technology, Bergen, Norway.*
Contact author: Nils Olav Handegard, Institute of Marine Research, PO Box 1870 Nordnes, 5817 Bergen, Norway, fax +47 55 23 85 31, email: nilsolav@imr.no

Introduction

Most fish generate thrust by bending their bodies into a backward-moving propulsive wave that extends to its caudal fin, a type of swimming classified as body and/or caudal fin (BCF) locomotion. Breder (1926) classified the BCF locomotion into five modes: anquiliform, sub-caragiform, carangiform, thunniform, and ostraciiform. The modes reflect changes mainly in the amplitude of the propulsive wave, but also in the way thrust is generated. For the carangiform Atlantic herring (*Clupea harengus* L.), the body undulations are confined to the last third of the body length, and thrust is provided by a rather stiff caudal fin.

The efficiency of fish swimming relies on the creation of vortices which generate extra inertia for the water around the tail. Like a spinning top that has sufficient inertia to stay upright, a small vortex of water has a tendency to stay in place. Breder (1965) hypothesized that schooling fish may collectively use each other's vortices, thus reducing the energy required to generate vortices for fish within the school. Herskin and Steffensen (1998) found that the tail-beat frequency (*F*; beats per second, bps) is lower at the rear of a school than in the front, indicating that energy savings occurs within schools.

To stay at a given depth, a fish needs to be neutrally buoyant, facilitated either by a swim bladder or a high body fat fraction. In addition to neutral buoyancy, the fish must maintain balance, which depends on the equilibrium of the forces of buoyancy and gravity. The fish can compensate for the non-neutral buoyancy or balance by extending their paired pectorals as hydrofoils (Alexander, 1971). Changing the form of the fins may increase the lift, similar to the flaps on an aerofoil. This requires more thrust to maintain speed, and results in a lower distance covered per tail beat (Videler, 1996, page 120).

Tracking fish targets with a split-beam echosounder is a mature method (e.g. Foote *et al.*, 1984 and 1986; and Ona, 1994), and estimating their positions and velocities are possible from the range and split-beam angles associated with the individual tracks. The method has been used to observe behaviour *in situ* (e.g. Huse and Ona, 1996; Torgersen and Kaartvedt 2001; Onsrud *et al.*, 2005, and Handegard and Tjøstheim, 2005). Estimates of *F* would complement the aforementioned information from traditional tracking methods.

Several methods exist to estimate *F*. Holiday (1974) measured the Doppler spread from three pelagic fish schools using 0.5 s 30 kHz CW pulses. The author then used Bainbridge's equation (Bainbridge,1958), which relates swimming speed to total length and *F*, to relate the Doppler spread at lateral sound incidence to fish swimming motion. Pincock and Easton (1978) reported a theoretical evaluation of Doppler shifts caused by tail beats to discriminate floating debris and fish targets, a typical problem in rivers. The idea has not, to our knowledge, been tested with real data. Continuous monitoring of *F* is also possible using tags attached to the fish. For example, Ross *et al.* (1981) used electromyography and acoustic telemetry to obtain data on *F*. Simpler non-intrusive tail-beat transmitters have also been developed (Lowe *et al.*, 1998). The advantage with these latter methods is that a single fish can be monitored.

Here, a newer method (Handegard, 2007) is further developed and tested, enabling measurements of *F* of several fish simultaneously. The main objective of this paper is to show how *F* can be estimated from variation in backscattering cross-sectional area (σ_{bs}; m^2) along a fish track, observed using a split-beam echosounder transmitting horizontally into a herring school.

Methods

Data were recorded using a horizontally projecting Simrad 38DD transducer lowered from the RV "Johan Hjort" into a dense herring layer at 245 m depth. The 38-kHz transducer has a, 7°-

beamwidth and is certified for use to 1500 m depth. The transducer was connected to a Simrad EK60 split-beam echosounder mounted aboard the ship through a 12.3 mm diameter armoured cable. A rudder mounted on the top of the transducer ensured that it did not rotate, and pointed directly into the weak fjord current. The vessel was completely darkened and drifted freely. The pulse length and repetition rate were 512 μs and 10 Hz, respectively, and target strength (*TS*; dB re 1 m^2) data were recorded for a range of 7 to 25 m. The echogram of *TS* uncorrected for the beam pattern and time-varied gain within individual targets (S_p; dB re 1 m^2) is presented in Figure 1. The duration of the data set is 2.7 min.

Trawl samples taken in the area consisted of herring (*Clupea harengus* L.) with a mean length L = 30.9 cm and standard deviation s.d. = 4.2 cm. The distribution was bimodal with distinct peaks at 27 cm and 34 cm. For further details, including calibration and biological sampling, see Pedersen *et al.*, this volume.

Individual targets were detected and tracked using an algorithm that associates pixels in the echogram to tracks (Handegard, 2007). The $\sigma_{bs}(t_p)$ for a track at time t and ping p along the track was estimated from the pixels associated with the track. Note that p=1 for the first sample in all tracks.

The split-beam samples were mapped to positions in Cartesian coordinates. A linear regression through all samples associated with a track was used to estimate the track position $\boldsymbol{x}$. Regressions were performed in each dimension with respect to time. The slopes of the regressions were used to estimate the mean velocity $\boldsymbol{v}$ and speed $v=|\boldsymbol{v}|$. The track velocity was corrected for along-axis currents by subtracting a 10 s running mean of all track's velocity components along the acoustic axis.

The resulting data set contained v, the estimated position vector $\boldsymbol{x}(t_p)$, and the backscattering cross section $\sigma_{bs}(t_p)$ for time t and ping p along the track. Track number, quality, and length were also output from an algorithm that compares forward and backward runs through the data set, calculating closeness to neighbours, and using phase jitter across a target at a given ping (Handegard, 2007, his equation (12)).

Model

Let θ_0 be the mean incident angle of an acoustic signal relative to a swimming fish. Assume that flexure of the fish body causes the actual incident angle relative to the swimbladder to fluctuate around the mean. Let the "true" incident angle be $\theta = \theta_0 + \Delta\theta$ where $\Delta\theta$ the perturbation is caused by the fish swimming. This is an approximation since the swimbladder also flexes and changes shape. Perturbations in incident angle were modelled simply as:

$$\Delta\theta = A\sin(2\pi tF), \tag{1}$$

where A is the amplitude of the tail-beat fluctuations. This assumes that the swim bladder is stiff and attached to two points at x = 0.3 and x = 0.5 along the fish centre line, where 0<x<1 is the position along the fish body (Figure 2a). The angle between the swim bladder position relative to the fish body is taken from Gorska and Ona (2003; Figure 2). The fish centreline, and the positions where the swim bladder is attached, is assumed to be displaced sideways according to:

$$\Delta y(x,t,F,L) = B(x)\cdot L\cdot\sin\left[2\pi\left(tF-\frac{x}{\lambda}\right)\right], \tag{2}$$

where $1/\lambda$ is the number of waves per body length, and $B(x)$ is an amplitude factor:

$$B(x) = \frac{\left(ax^2 + bx + c\right)}{100}. \quad (3)$$

The parameters used are L = 0.32 m, λ = 1.031 m, a = 0.173, b = -1.22, and c = 3.1. The model parameters are typical values for a sub carangiform swimming mode, given the aforementioned model assumptions [pers. comm. William Thielicke, parameters derived from Videler (1996)]. The angle $\Delta\theta(t, F, L)$ is derived from the slope of the linear curve between the points $[0.3L, \Delta y(0.3, t, F, L)]$ and $[0.5L, \Delta y(0.5, t, F, L)]$. Setting A =4 deg, the largest residual between Equation (1) and this assumed fish/swim bladder model is less than $2 \cdot 10^{-2}$ deg, indicating that Equation (1) is an appropriate approximation.

Several models exist to relate acoustic backscatter to incident angle (e.g. Simmonds and MacLennan, 2005). Here the Kirchoff-ray mode model (Clay and Horne, 1996) and the composite scattering model (Chu *et al*., 2006) are used to estimate the acoustic backscatter as a function of incident angle θ and length L. Combined with typical herring swimbladder dimensions (Gorska and Ona, 2002), approximations to the acoustic backscatter are obtained (see Figure 2b)**:**

$$\sigma_{bs} = f(\theta, L). \quad (4)$$

Combining Equations (1) and (4), σ_{bs} is estimated as a function of F and L. However, the periodogram varies in complex ways, depending on the aspect of ensonification, as the effects of the tail create perturbations around that aspect. Rather than using the model for exact mappings from σ_{bs} to $\Delta\theta$, and then performing spectral analysis on $\Delta\theta$, the model is used to define intervals in θ_0 where the periodogram of σ_{bs} is directly related to F. To be directly related, σ_{bs} must increase or decrease monotonically in the interval $[\theta_0 - A \;\; \theta_0 + A]$. If the slope is negative (i.e. σ_{bs} decreases with increasing θ), the phase of σ_{bs} is shifted 180 deg relative to $\Delta\theta$ (Figure 2c). As an approximation, the phase is shifted 180 deg when $\theta_0 > \frac{\pi}{2}$. This has implications when comparing the phase between adjacent tracks. When the relationship is not monotonically increasing or decreasing, multiple peaks may occur within a period and any detected period in σ_{bs} may be harmonics of F (Figure 2d).

Analysis

Assuming F is directly related to the periodicity of $\sigma_{bs}(t_p)$, the periodogram is used to directly estimate F. Instead of using σ_{bs}, the backscatter length $\sqrt{\sigma_{bs}(t_p)}$ is used to generate the periodogram. Before estimating the periodogram, tracks of length less than 40 pings are removed before further analysis. Missing data were replaced by linearly interpolated values to retain a fixed sample rate. In this data set, 6% of the values were interpolated. The periodogram of $\sqrt{\sigma_{bs}(t_p)}$ was estimated using a 128-point Fast Fourier Transformation (FFT) algorithm (Based on Frigo *et al.* 1998, implemented in Matlab, MathWorks Inc.). Let J_j be the FFT of $u_p \cdot x_p$, where $x_p = \sqrt{\sigma_{bs}(t_p)} - \overline{\sqrt{\sigma_{bs}}}$, σ_{bs} is the backscatter along the track, overbar denotes mean along the track, and u_p is the weight used to taper the series.

The taper weights were calculated using a cosine bell on 50% of the data [Bloomfield, 1976, his Equation (9)], primarily to reduce leakage between frequencies. The series were zero-padded when shorter than 128-points, and truncated when longer. A fixed length was used to estimate the same Fourier frequencies for each track, enabling inter-track comparisons. After computing the FFT, periodograms were estimated as $I_j = J_j J_j^*$, where * indicates the complex conjugate.

Ensemble average

Estimating *F* for a single track requires high quality data; therefore, manually scrutinizing the data is necessary. This is tedious and time consuming. Assuming similar behaviour between individuals, the ensemble average is calculated between individuals as:

$$\mathrm{I_j} = \frac{1}{\mathrm{N}} \sum_{\mathrm{i=1}}^{\mathrm{N}} \mathrm{I_{j,m}} \,, \tag{5}$$

where $I_{j,m}$ is the periodogram for track *m* and Fourier frequency *j*, and *N* is the number of tracks. This is possible since similar Fourier frequencies have been used for all tracks. Both low and high quality tracks were included to get an indication of the sensitivity to low quality tracks for $\overline{I_j}$. If not sensitive, the requirements for the manual scrutiny can be relaxed.

Cross periodogram of nearest neighbour

An interesting aspect of estimating *F* is its relation to the (assumed) nearest neighbour. An algorithm that detects the nearest targets based on the ***x***-positions was used, and a well-defined high-quality pair was visually chosen as an example. The amplitude of the cross-periodogram for the *j*th Fourier frequency, between track *m* and *n*, is calculated as in Bloomfield (1976, page 211):

$$\left| I_{m,n,j} \right|^2 = I_{j,m} I_{j,n} \,. \tag{6}$$

If the series from track *m* were on the form:

$$x_{m,p} = R_m \exp\left[i\left(\lambda p + \phi_m \right) \right], \tag{7}$$

then the FFT would be:

$$I_{m,j} = R_m \exp\left(i \phi_m \right), \tag{8}$$

and similarly for track *n*. The cross-periodogram would then be:

$$I_{m,n,j} = \frac{n}{2\pi} R_m R_n \exp\left[i\left(\phi_m - \phi_n \right) \right], \tag{9}$$

with relative phase $\phi_m - \phi_n$. When the series contains a strong periodicity, the relative phase at that frequency gives the phase difference between the two series. When the mean incident angle θ_0 has a negative slope (Figure 2c), the phase difference is shifted 180 deg. For the low values in $\left| I_{m,n,j} \right|$, the relative phase has no meaning.

Results

The echogram with appropriately set colour scale (Figure 1a), shows periodicity in some of the tracks. Details of the two adjacent tracks in Figure 1b, shows the periodicity more clearly. The peaks and troughs can be counted by eye, and F can be roughly estimated. However, some tracks exhibit variable F, not all tracks exhibit strong periodicity, and some do not show any sign of periodicity. The track in Figure 1d starts with a periodicity and transitions to a smooth track towards the end, probably associated with a swim-glide behaviour.

A result of the automated tracking algorithm used to associate pixels to tracks is given in Figure 1c. Track B bleeds into track A as a consequence of erroneous associations from the tracking algorithm. This shows that the results from automated tracking algorithms must be critically inspected. This error was kept in the following analysis to obtain an idea of the robustness of the whole procedure.

The overlapping part of $\sqrt{\sigma_{bs}}$ along tracks A and B (Figure 1b) is shown in Figure 3a. Again, the periodicity is clearly seen, although the signal is somewhat garbled at the beginning of the track, probably caused by mis-association in the tracking algorithm. In Figure 3b**,** both periodograms show distinct peaks, at 1.24 Hz and 1.32 Hz for tracks A and B, respectively, indicating that F is similar between the tracks.

The relative phase from the three strongest cross-periodogram peaks are shown in Figure 3c, showing a relative phase difference of approximately 90 deg. The mean incident angle θ_0 for track A is 159 deg and for track B is 161 deg. Consequently, the phases are shifted 180 deg for both tracks. The estimated track positions $\boldsymbol{x}$ are shown in Figure 3d.

Manually tracking data is tedious and less consistent than automated tracking, but the quality may be better. The mean periodogram $\overline{I_j}$ of all detected tracks is presented in Figure 4a. A distinct peak at 1.4 Hz is seen. Note also the high energy in the low frequencies. Finally, the estimated speed as a function of F is presented for the two example tracks and for the whole data set (Figure 4b).

Discussion

Method

These results agree those from previous studies relating swimming speed and F (Videler, 1996, his Figure 6.1; Steinhausen *et al.*, 2006, their Figure 2), and are also consistent with those presented in Ross *et al.* (1981, i.e. F rarely exceeded 2.5 bps). The ensemble-average periodogram estimates the mean F, even without constraining the analysis to high quality tracks, indicating that the method is robust.

The relationship between θ and swimming is more complex than our simple model indicates, and so is the real backscatter from a swimming fish. This complexity is more pronounced for higher acoustic frequencies (e.g. Burwen *et al.*, 2007), and increasing the frequency will probably lead to fewer detections over larger ranges of θ (e.g. Figure 2d). Accurately quantifying these ranges requires a sophisticated model, but instead we accept their existence and in that accept that higher harmonics and other distortions in the estimates of F may occur. The strength of the higher harmonics may give an indication of the importance of this effect. A detailed inspection of Figure 4a shows that energy at 2.5 Hz. This may be contributed from harmonics, but it could also be caused by other factors like artefacts from the tapering and padding. In any case, this effect is not pronounced in this analysis, but

should be kept in mind when using this method for other acoustic frequencies, fish lengths or species.

As seen in Figure 4a, the ensemble average contains a strong low frequency component. This component may be caused by slow changes in swimming direction, causing a low frequency component in the σ_{bs}. When we removed a fitted 2nd order polynomial instead of the mean from $\boldsymbol{x}_p$, this component was reduced for the ensemble average (Figure 4a, grey curve). This indicates that slow changes in σ_{bs}, caused by changes in swimming direction, for example, may cause low frequency components to appear in the periodogram. However, this is not seen in the high quality tracks in Figure 3, and that may be an indication that it is an artefact of the tracking algorithm caused by the low quality tracks, rather than changes in swimming behaviour.

Other sources of error can be related to the instrument setup, like strumming of the cable causing the orientation of the beam to shift. The expected strum frequency can be similar to the detected *F*. However, smooth tracks, tracks with a periodicity, and tracks with different phases are found in close proximity, within the same pings, indicating that the periodicity is not likely to be caused by the instrument.

Estimating position and velocity with a split-beam echosounder is a well established method, but there are some pitfalls. For automatic tracking, the process of associating targets to tracks may be erroneous (Figure 1c). This error may cause jumps in the positions and swimming velocities to be grossly overestimated. Also, a low signal to-noise ratio can potentially cause bias in the split-beam angles (Demer *et al.*, 1999; Kieser *et al.*, 2000), which in turn leads to bias in the position and velocity estimates. For the tail-beat estimation method, the consequence is less severe since we do not rely on the split-beam angles. The erroneous association leads to more difficult estimation of the periodogram, but not large biases as in the estimated velocities. This seems reasonable when comparing the estimate of *F* from the ensemble average to that of the high quality tracks (Figures 3b and 4a). Recall that these tracks had erroneous associations.

Potential of the method

F can be related to the swimming velocity, which is associated with an energetic cost (Webb, 1975). Models exist where this energetic cost is set in an evolutionary perspective (Strand and Huse, 2007), and our method can provide valuable data to those kinds of models, simply by calculating the robust ensemble average at different depths.

The fat deposit varies over season and age. This causes changes in the required thrust with fish condition due to its impact on both buoyancy and balance (Ole Brix, Pers. Comm.). If the fish adjust their pectoral fins to maximize lift, the increase in drag will cause a reduced stride length (Videler, 1996, page 120). The stride length can then be estimated from simultaneous observations of swimming speed and tail-beat frequency. It is then possible that changes in stride length over season can provide an indicator of fish condition, and that this may be observed *in situ* using a probing echosounder. This also has implications for tilt angle distributions, an important parameter relating modelled and observed *TS* (Simmonds and MacLennan, 2005).

When swimming velocity, position, and *F* can be reliably estimated for each track, the inter-individual behaviour can be analyzed. This may aid the parameterization of traditional schooling models (Parr, 1927; Aoki, 1982; Reynolds, 1987). The possibility to observe the relative phase in *F* among individuals within in a school is original. Since the relative position to the assumed nearest neighbour is estimated, the relative phase in a field around the fish may be mapped. We can gain insight into how the swimming phase around the fish may be

adjusted to take advantage of vortexes in the school. Our method has the potential to do these observations *in situ*.

Observing *F* is a standard procedure in *ex situ* experiments, but is more difficult to obtain *in situ*. We have shown that a relatively simple approach can provide reliable estimates of *F in situ* using a probing echo sounder.

Acknowledgements

We are grateful to Egil Ona for useful discussions. We thank the Norwegian Research Council for financial support under the strategic institute program "EcoFish".

References

Alexander, R.M. 1971. Size and Shape. Arnold, London. 59 pp.

Aoki, I. A Simulation Study on the Schooling Mechanism in Fish. 1982. Bulletin of the Japanese Society of Scientific Fisheries,48: 1081-1088.

Bainbridge, R. 1958. The Speed of Swimming of Fish as Related to Size and to the Frequency and Amplitude of the Tail Beat. Journal of Experimental Biology, 35: 109-133.

Bloomfield, P. 1974. Fourier analysis of time series: An introduction. Wiley & Sons, New York. 258 pp.

Breder, C.M. 1926. The locomotion of fishes. Zoologica, 4: 159-256.

Breder, C.M. Jr. 1965, Vortices and fish schools. Zoologica, 50: 97-114.

Burwen, D.L.; Nealson, P.A.; Fleischman, S.J.M. & Horne, J.K. 2007. The complexity of narrowband echo envelopes as a function of fish side-aspect angle ICES Journal of Marine Science, 64: 1066-1074.

Chu, D., Stanton, T. K., Jech, J. M., and Reeder, D. B. 2006. Modeling of the backscattering by swimbladder-bearing fish. Journal of the Acoustical Society of America, 120(5): 3105-3105.

Clay, C.S. and Horne, J.K. 1994. Acoustic Models of Fish - the Atlantic Cod (*Gadus Morhua*). Journal of the Acoustical Society of America, 96(3): 1661-1668.

Demer, D. A., Soule, M.A. and Hewitt, R.P. 1999. A multiple-frequency method for potentially improving the accuracy and precision of *in situ* target strength measurements. Journal of the Acoustical Society of America, 105(4): 2359-2376.

Foote, K. G., Aglen, A., and Nakken, O. 1986. Measurement of fish target strength with a split-beam echo sounder, Journal of the Acoustical Society of America, 80: 612–621.

Foote, K. G., Kristensen, F. H., and Solli, H. 1984. Trial of a new, splitbeam echo sounder. ICES Document CM 1984/B:21. 15 pp.

Frigo, M. and Johnson, S. G. 1998. FFTW: An Adaptive Software Architecture for the FFT. Proceedings of the International Conference on Acoustics, Speech, and Signal Processing, 3: 1381-1384.

Gorska, N. and E. Ona, E. 2003. Modelling the effect of swimbladder compression on the acoustic backscattering from herring at normal or near-normal dorsal incidences. ICES Journal of Marine Science, 60(6): 1381-1391.

Handegard, N.O. and Tjøstheim, D. 2005. When fish meets a trawling vessel: examining the behaviour of gadoids using a free floating buoy and acoustic split-beam tracking. Canadian Journal of Fisheries and Aquatic Sciences, 62: 2409-2422.

Handegard, N.O. 2007. Observing individual fish behavior in fish aggregations: Tracking in dense aggregations. The Journal of the Acoustical Society of America, 122: 186.

Herskin, J. & Steffensen, J.F. 1998. Energy savings in sea bass swimming in a school: measurements of tail beat frequency and oxygen consumption at different swimming speeds. Journal of Fish Biology, 53: 366-376.

Holliday, D. V. 1974. Doppler structure in echoes from schools of pelagic fish. The Journal of the Acoustical Society of America, 55: 1313-1322.

Huth, A. and Wissel, C. 1992. The Simulation of the Movement of Fish Schools. Journal of theoretical biology, 156: 365-385.

Huse, I. and Ona, E. 1996. Tilt angle distribution and swimming speed of overwintering Norwegian spring spawning herring. ICES Journal of Marine Science, 53: 863-873.

Kieser, R., Mulligan, T. and Ehrenberg, J. 2000. Observation and explanation of systematic split-beam angle measurement errors. Aquatic Living Resources, 13: 275-281.

Lowe, C.G., Holland, K.N. and Wolcott, T.G. 1998. A new acoustic tailbeat transmitter for Fishes. Fisheries Research, 36: 275-283.

Onsrud, M., Kaartvedt, S. and Breien, M. 2005. *In situ* swimming speed and swimming behaviour of fish feeding on the krill *Meganyctiphanes norvegica*. Canadian Journal of Fisheries & Aquatic Sciences, 62: 1822–1832.

Ona, E. 1994. Recent developments of acoustic instrumentation in connection with fish capture and abundance estimation, in *Marine Fish Behaviour in Capture and Abundance Estimation*, edited by A. Fernö and S. Olsen. Fishing News Books, Oxford, UK, pp. 200–214.

Parr, A.E. 1927. A contribution to the theoretical analysis of the schooling behaviour of fishes. Occasional papers of the Bingham collection, 1: 1-32.

Pincock, d.G. & Easton, N.W. 1978. The feasibility of Doppler Sonar Fish Counting IEEE Journal of Oceanic Engineering, OE-3: 37-40.

Reynolds, C.W. 1987. Flocks, Herds, and Schools: A Distributed Behavioural Model. Computer Graphics, 21: 25-34.

Ross, L., Watts, W. and Young, A.H. 1981. An ultrasonic biotelemetry system for the continuous monitoring of tail-beat rate from free-swimming fish. Journal of Fish Biology, 18: 479-490.

Simmonds, E. J. and MacLennan, D. N. 2005. Fisheries Acoustics: Theory and Practice, Blackwell Publishing, London. 437 pp.

Strand, E. and Huse, G. 2007. Vertical migration in adult Atlantic cod (*Gadus morhua*). Canadian Journal of Fisheries & Aquatic Sciences, 64: 1747-1760

Steinhausen, M. F., Steffensen, J. F. and Andersen, N. G. 2005. Tail beat frequency as a predictor of swimming speed and oxygen consumption of saithe (*Pollachius virens*) and whiting (*Merlangius merlangus*) during forced swimming. Marine Biology, 148: 197-204

Torgersen, T. and Kaartvedt, S. 2001. *In situ* swimming behaviour of individual mesopelagic fish studied by split-beam echo target tracking. ICES Journal of Marine Science, 58: 346-354

Videler, J. 1993. Fish Swimming. Chapman & Hall, London. 260 pp.

Webb, P. W. 1975. Hydrodynamics and energetics of fish propulsion. Bulletin (Fisheries Research Board of Canada), 190. 158 pp.

Figure captions

Figure 1. (a) The echogram (S_p; dB; time-varied-gain=40log(r), r = range (m)) from the horizontally projecting transducer at 245 m. The white boxes indicate the position of the detailed echograms in b and d. (b) Two adjacent well-defined tracks were used to demonstrate cross-periodogram estimation. (c) Associations between samples and the tracks in the echogram (b), including some erroneous associations due to the tracking algorithm. (d) A single track showing swim-glide behaviour.

Figure 2. (a) The model of a swimming fish, shown for t = 3 s, F = 1.7 Hz, and L = 32 cm. The asterisks, which denote the endpoints of the swim bladder, are located at $\left[0.3L \;\; \Delta y(x=0.3)\right]$ and $\left[0.5L \;\; \Delta y(x=0.5)\right]$. The slope between these points is used to calculate $\Delta\theta$. The angles θ_0 and θ are indicated by the inner and outer arc, respectively. The centreline of the fish is modelled simply as Δy as a function of x (Equation (1)). The inner and outer shapes are assumed to be outlines of the fish and swim bladder, respectively (for visualization only). (b) $TS = 10\log(\sigma_{bs})$ as a function of θ for the Kirchoff-ray mode model (Clay and Horne, 1996) (black line), and the composite scattering model (Chu *et al.*, 2006) (grey line). (c, d) The expected variation in TS (grey line) and θ (black line) as a function of t for $\theta_0 = 110$ deg and $\theta_0 = 42$ deg, respectively.

Figure 3. (a) The $\sqrt{\sigma_{bs}}$ along two adjacent tracks. The black and grey lines are the overlapping parts of tracks A and B in Figure 1b, respectively. (b) The periodogram for the two tracks. (c) The relative phases between the two tracks for the three strongest components in the cross periodogram. Here we ignore the low frequency components. The relative phase is the angle from the centre to the +; and the distance from origin indicates the relative strength of the cross-spectrum for that F. The F is indicated by the numbers adjacent to each point. (d) The position of the two adjacent tracks estimated by linear regression through the split-beam samples. The + corresponds to ping number 1443, and the ∇ indicates ping 1508, respectively (i.e. the start and stop of the two tracks).

Figure 4. (a) The mean periodogram over all tracks. The grey line visible up to 1 Hz is the periodogram where a fitted 2nd order polynomial was subtracted, instead of the mean, prior to the FFT. (b) Swimming speed in Ls^{-1} vs. estimated F. The error bar denotes the mean and empirical s.d. for the estimated swimming speeds for all tracks in the test data, plotted at the peak frequency of 1.4 Hz. The * are the data points from the tracks A and B in Figure 2. The grey line is the regression line taken from Videler (1996, Figure 6.1), and the black curve is the regression line from Steinhausen *et al.* (2006, Figure 2).

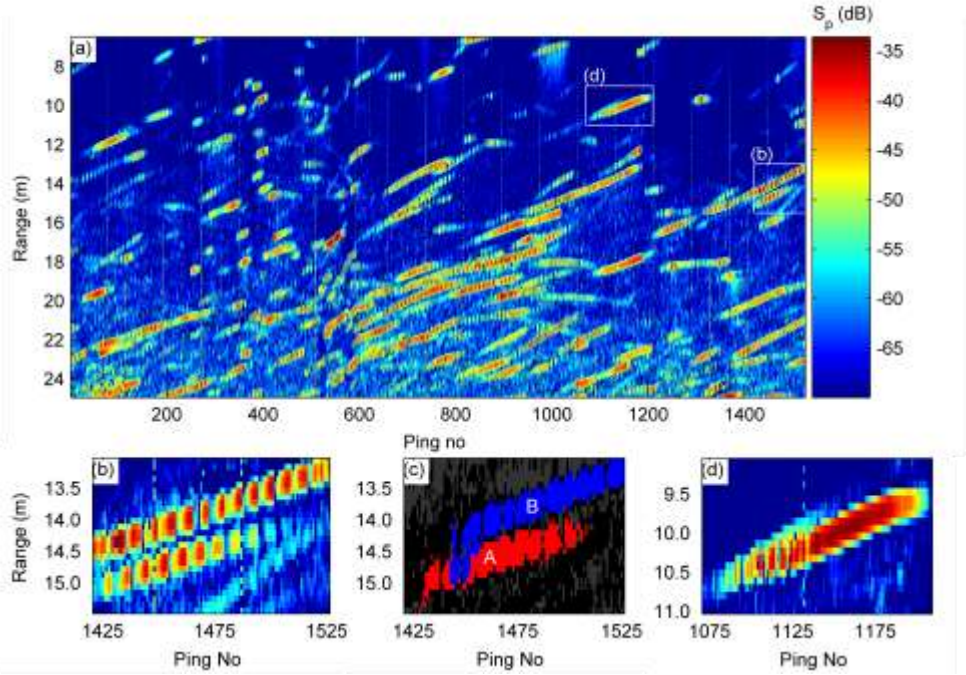

Figure 1.

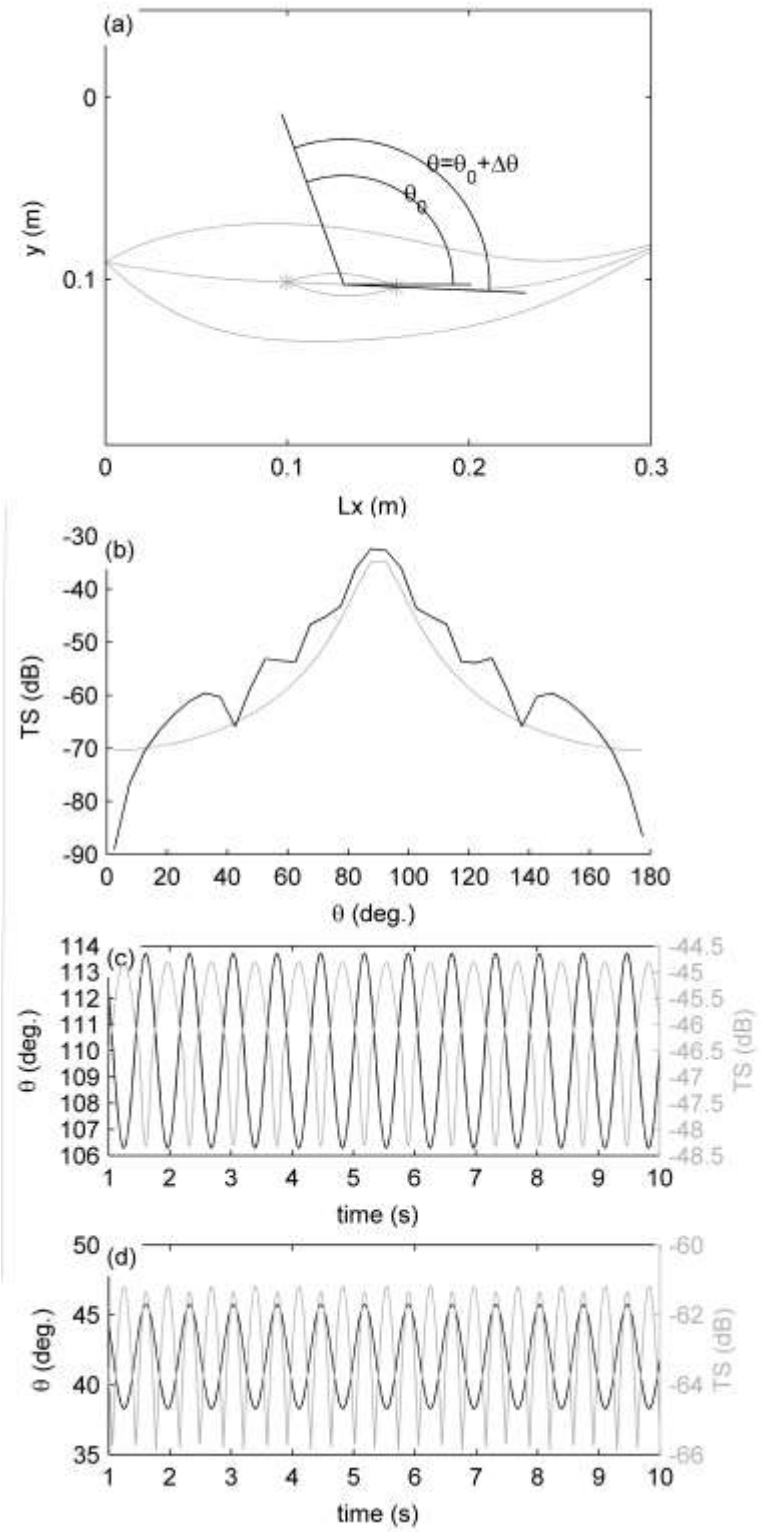
(a)
θ=θ0+Δθ
θ0
y (m)
Lx (m)
(b)
TS (dB)
θ (deg.)
(c)
θ (deg.)
TS (dB)
time (s)
(d)
θ (deg.)
TS (dB)
time (s)

Figure 2.

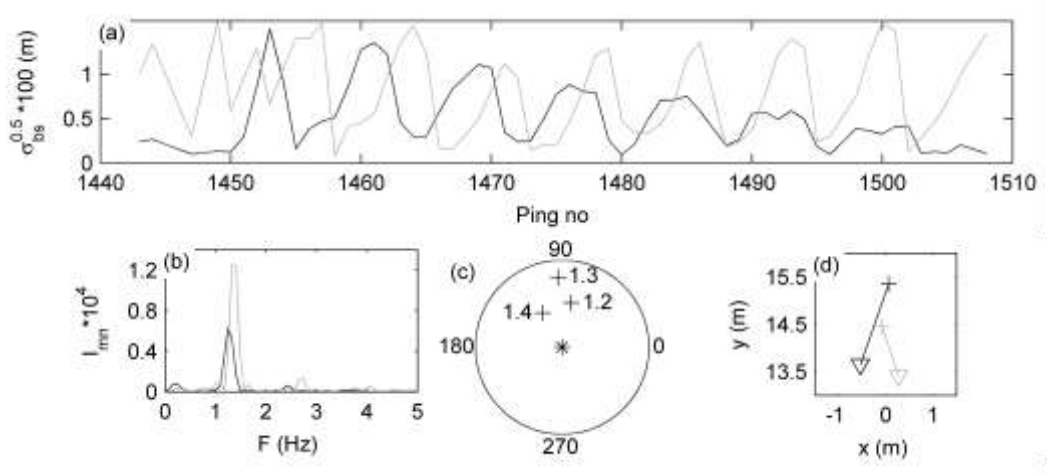
(a)
$\sigma_{bs}^{0.5}$ *100 (m)
1
0.5
0
1440
1450
1460
1470
1480
1490
1500
1510
Ping no
(b)
I_{mn} *10^4
1.2
0.8
0.4
0
0
1
2
3
4
5
F (Hz)
(c)
90
+1.3
+1.2
1.4+
180
0
270
(d)
15.5
14.5
13.5
y (m)
-1
0
1
x (m)

Figure 3.

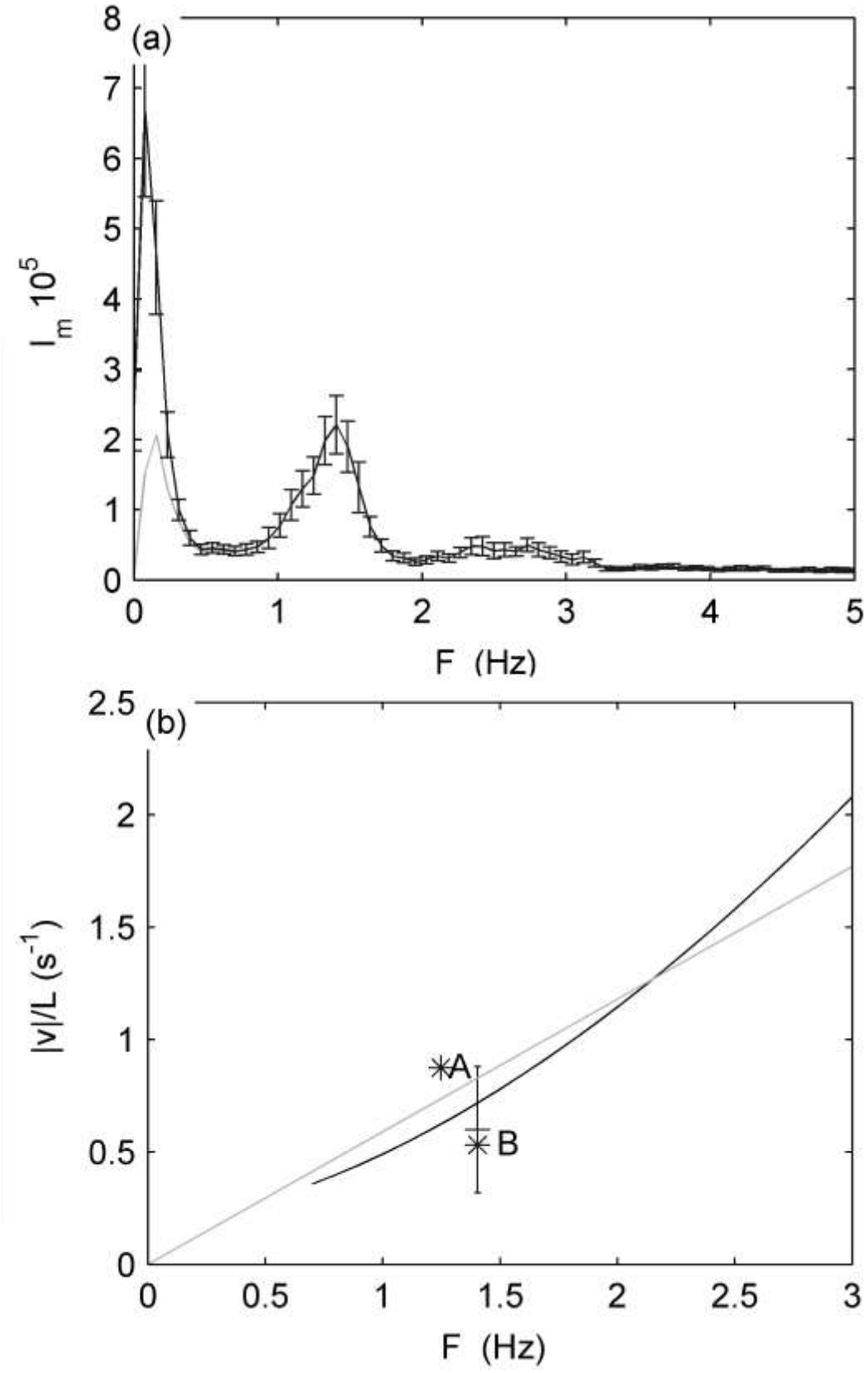

Figure 4.